## *Supplementary Information*

*for*

# Atomically distributed asymmetrical five-coordinated Co-$N_5$ moieties on N-rich doped C enabling enhanced redox kinetics for advanced Li-S batteries

Fanchao Zhang, Zihuan Tang, Tengfei Zhang, Hong Xiao, Huifeng Zhuang, Xiao Liang, Lirong Zheng* and Qiuming Gao*

## *Table of Contents*

## *Experimental Procedures*

### *Synthesis of CoN5 SA/NC*

In a typical procedure, commercial carbon blacks (Vulcan XC-72) were refluxed in a 9 M nitric acid solution at 90 °C for 3 h to obtain activated carbon black (AC) support. Cobalt acetate tetrahydrate (19.9 mg) and 1,10-phenanthroline monohydrate (111.0 mg) were added into 30 mL of ethanol and then stirred for approximately 30 min at room temperature. Then 150 mg of ACs was added into the above solution followed by sonicated for 1 h to obtain a black suspension, and the mixture was kept under magnetic stirring for 12 h. The resultant precipitate was collected via solvent evaporation at 65 °C and dried under a vacuum. Afterward, the black precipitate was mixed with urea with a mass ratio of 1:10, then the powders were annealed at 600 °C for 2 h under $N_2$ flow. After cooling to room temperature, the final product (CoN5 SA/NC) was obtained. The Co-NC and NC samples were obtained using a similar fabrication process, except that the absences of urea and Co precursor, respectively. The Co-C was prepared using a similar procedure, except that 1,10-phenanthroline monohydrate and urea were absent.

### *Material characterization*

Powder X-ray diffraction (XRD) patterns of the samples were recorded on an X-ray diffractometer (Rigaku D/max2200PC) with Cu Kα (λ = 0.15418 nm) radiation source and scanning range of two-theta angle changes from 10° to 80°. The morphologies and structures were surveyed by high-resolution transmission electron microscopy (HRTEM, JEOL 2100F) and a field-emission scanning electron microscope (FESEM, JEOL, JSM7500). The double-aberration-corrected high-angle annular dark-field scanning (HAADF-STEM) images and EDX elemental maps were obtained on a JEM-ARM300F with an acceleration voltage of 300 kV. Chemical compositions and states were surveyed by X-ray photoelectron spectroscopy (XPS, Thermo Scientific, ESCALAB 250 XI+). Raman spectra were collected on a Jobin Yvon (Laboratory RAM HR800) with a 633 nm laser wavelength. Specific surface area and pore distribution of the samples were calculated by Brunauer-Emmett-Teller (BET, American Micromeritics ASAP 2010). The concentrations of all the catalysts were measured by inductively coupled plasma optical emission spectrometer (ICP-OES, Agilent 725). X-ray absorption fine structure (XAFS) spectra of Co K-edge containing the X-ray absorption near edge-structure (XANES) and extended X-ray absorption fine structure (EXAFS) were obtained at the 1W1B station of Beijing Synchrotron Radiation Facility, P. R. China. The data were performed in fluorescence mode using a Lytle detector.

### *Fabrication of functional separator*

The functional separators were commercial polypropylene (PP) separator (Celgard-2500) coated with electrocatalyst layer via typical vacuum filtration. Specifically, the as-synthesized CoN5 SA/NC, CNT and polyvinylidene difluoride (PVDF) with a weight ratio of 8:1:1 were dispersed in N, N-Dimethylformamide (DMF) solvent under sonication procedure. After that, the samples were filtered on PP separator to acquire the CoN5 SA/NC modified separator. The CoN5 SA/NC modified separator was dried under vacuum at 60 °C for 12 h, which was then punched into discs with a diameter of 19.0 mm. Reference samples were prepared through similar procedures except that CoN5 SA/NC was replaced by NC, Co-C and Co-NC, respectively.

### *Electrochemical measurements*

The sulfur loading of regular sulfur cathode is *ca.* 1.2 $mg_S$ $cm^{-2}$ in a CR2032-type coin cell. Typically, the cathode was prepared by mixing 80 wt% sulfur/CNT (weight ratio = 3:1), 10 wt% PVDF and 10 wt% acetylene black via ball-milling in N-methyl-2-pyrrolidone (NMP) solvent for 3.0 h to generate a homogenous slurry. After that, the obtained slurry was casted onto the Al foil collectors, and dried under vacuum at 60 °C for 12 h. The cathode samples were punched into discs with area of 1 $cm^2$ to assemble in coin cells. Especially, the sulfur high loading is 5.0-7.0 $mg_S$ $cm^{-2}$ for the sulfur/carbon/catalyst cathodes, which were fabricated through similar procedures except that acetylene black was replaced by CoN5 SA/NC. The electrolyte was 1.0 M lithium bis(trifluoromethanesulfonyl)imide (LiTFSI) and 2.0 wt% of $LiNO_3$ additive in a solvent of 1,3-dioxolane (DOL) and 1,2-dimethoxyethane (DME) (v/v = 1:1). The ratio of electrolyte to sulfur in the cathode was *ca.* 20 μL $mg^{-1}$ for the regular electrodes. The Li-S cells were measured by LAND-CT2001A battery testing system with a voltage range of 1.7-2.7 V. The cells used for cyclic voltammetry (CV) and electrochemical impedance spectroscopy (EIS) experiments were performed on a CHI660D electrochemical workstation. The CV curves were recorded in the voltage between 1.6 and 2.8 V at a scan rate range of 0.1-0.5 mV $s^{-1}$. The EIS spectra were recorded in the frequency range from 100 kHz to 0.1 Hz at a sinusoidal excitation voltage of 5 mV.

### *Polysulfide-adsorption test*

The sublimed sulfur and anhydrous lithium sulfide (molar ratio = 5:1) were dissolved in mixture of DOL/DME (v/v = 1:1) solvent, and vigorously stirred for about 24 h in an Ar-filled glove box to prepare $Li_2S_6$ solution (5 mM). Then 20 mg of CoN5 SA/NC, Co-NC, Co-C and NC samples were dispersed in about 2.5 mL of the as-prepared $Li_2S_6$ solutions, respectively. After being shaken and keep standing for 8 h, the optical phenomena could be taken optical photos. Further, the supernatant and the sediment were separated to be tested for UV-vis and XPS spectra, respectively.

### *Symmetrical cell assembly and measurement*

The electrodes for symmetric cells were fabricated by uniformly mixing active materials with PVDF at a weight ratio of 4:1 in NMP and cast onto the Al foil collectors. The electrodes were punched into discs with area of 1 cm2 used as cathode and anode to assemble the symmetrical cells. 40 μL of 0.25 M $Li_2S_6$ solution and Celgard-2500 membrane were employed as electrolyte and separator, respectively. The CV measurements of the symmetric cell were conducted between -1.0 and 1.0 V at a scanning rate of 5 mV $s^{-1}$.

### *Potentiostatic nucleation of $Li_2S$*

The active materials of the cathodes were coupled with Li foil anodes to assemble the coin-cells, and the electrolytes contain 0.25 M $Li_2S_8$, 1 M LiTFSI, and 2.0 wt % $LiNO_3$. Firstly, the fabricated Li-$Li_2S_8$ cells were galvanostatically discharged to 2.12 V under 0.112 mA, and then kept potentiostatically at 2.05 V until the current was lower than $10^{-2}$ mA. The nucleation capacity of $Li_2S$ can be figured out by the integral area of the plotted curve through Faraday's law.

### *Density functional theory (DFT) calculations*

All calculations were carried out based on DFT as implemented in Vienna ab initio simulation package (VASP) with exchange-correlation function of generalized gradient approximation (GGA) of Perdew, Burke, and Ernzerhof (PBE) method. A grid of 3 × 3 × 1 Monkhorst-Pack k-points was used for the structural relaxation. A vacuum layer of 15 Å is adopted in the direction perpendicular to the monolayer surface to avoid the interactions between periodic slabs. The energy cutoff was set to be 500 eV. The convergence criterion for the energy and maximum force for the optimization were set to 10-5 eV and 0.05 eV/Å, respectively. To further explain the relative reaction trend of $Li_2S_n$ and $S_8$ species, the free energy changes are calculated according to the following equation (S1):

$$\Delta G = \Delta E + \Delta E_{ZPE} - T\Delta S \tag{S1}$$

where, $\Delta E$, $\Delta E_{ZPE}$, and $\Delta S$ represent the differences of total energy, zero-point energy, and entropy between the product and reactants, respectively. Here, we just consider the ground states of S-containing species at temperature of 0 K. So, the contribution from the entropy term is zero.

***Supplementary Figures***

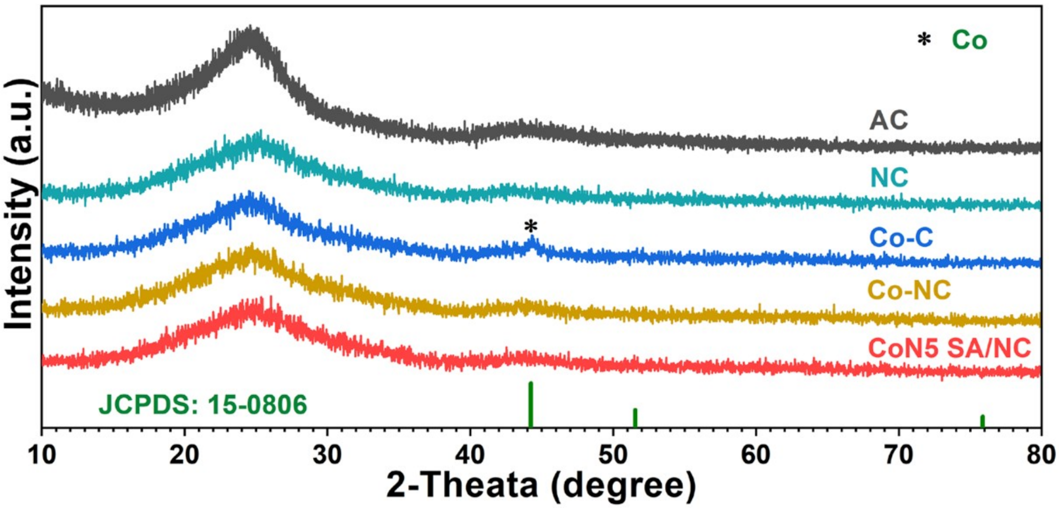

**Fig. S1.** Powder XRD patterns of CoN5 SA/NC, Co-NC, Co-C, NC, and AC.

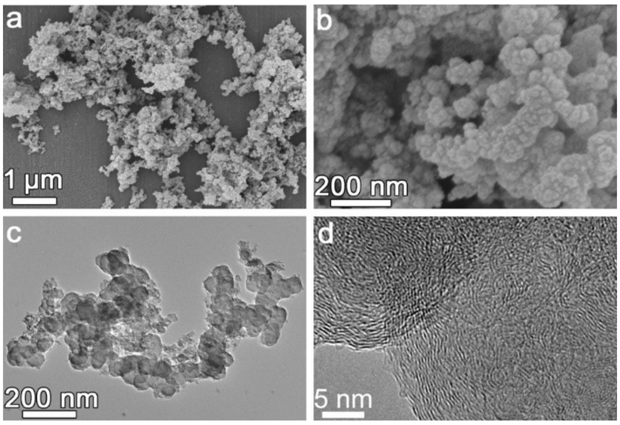

**Fig. S2.** (a,b) SEM, (c) TEM and (d) HR-TEM images of CoN5 SA/NC.

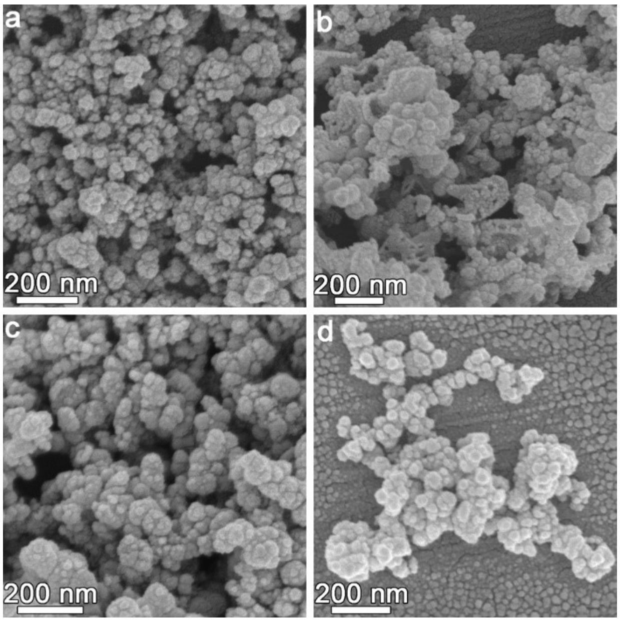

**Fig. S3.** SEM images of (a) AC, (b) NC, (c) Co-C and (d) Co-NC.

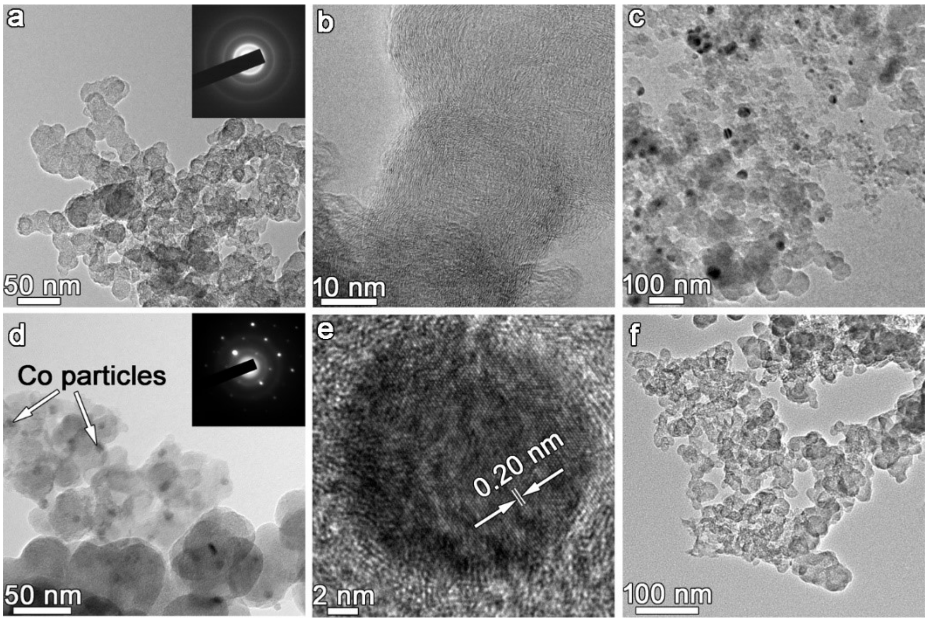

**Fig. S4.** (a) TEM image, SAED pattern (inner) and (b) HRTEM of Co-NC. (c,d) TEM with insert of the SAED pattern and (e) HR-TEM image of Co-C. (f) TEM image of NC.

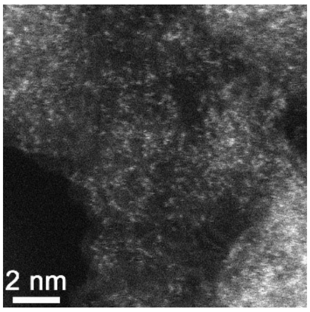

**Fig. S5.** HAADF-STEM image for CoN5 SA/NC.

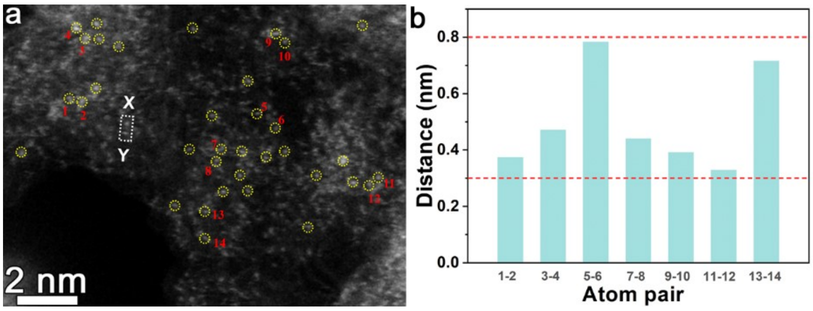

**Fig. S6.** (a) HAADF-STEM image and (b) Atomic spacing distribution diagram (atoms marked by red numbers in Fig. S6a).

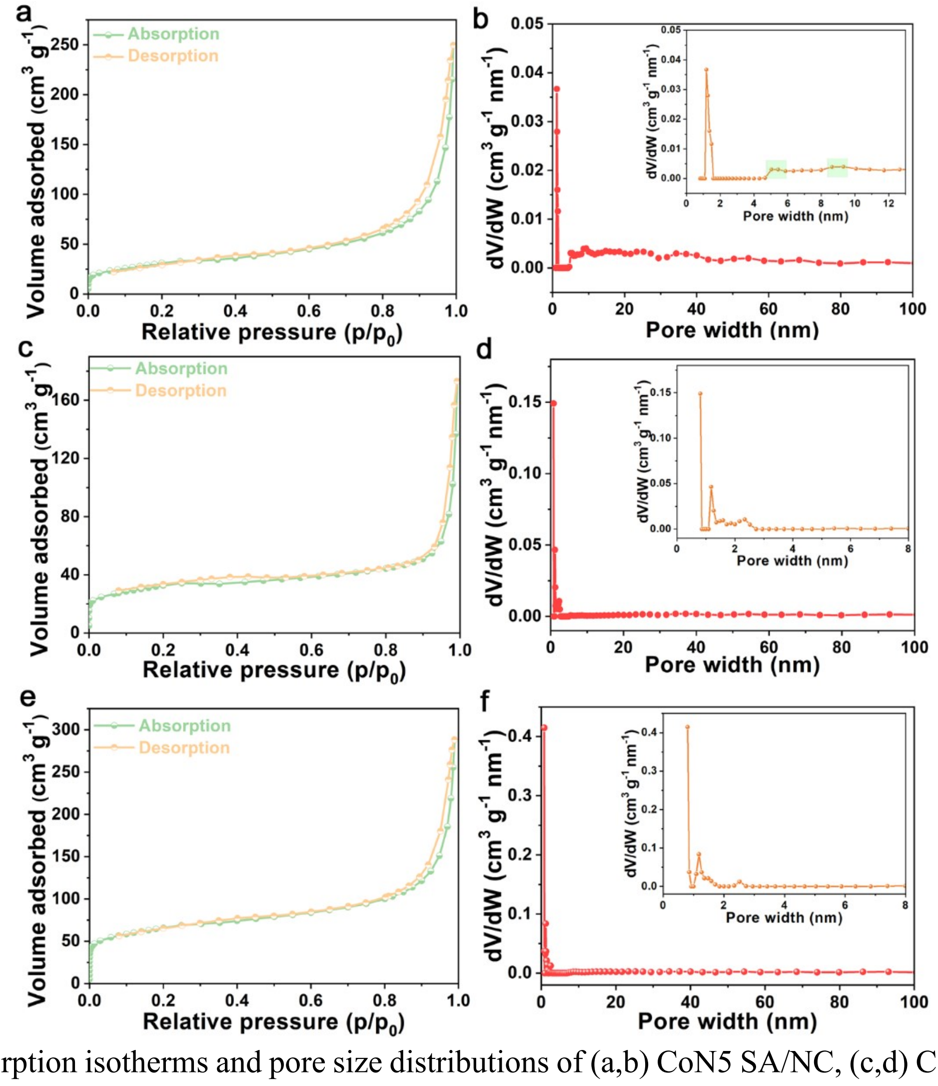

**Fig. S7.** $N_2$ sorption isotherms and pore size distributions of (a,b) CoN5 SA/NC, (c,d) Co-NC and (e,f) AC. Pore size distributions are calculated by density functional theory (DFT).

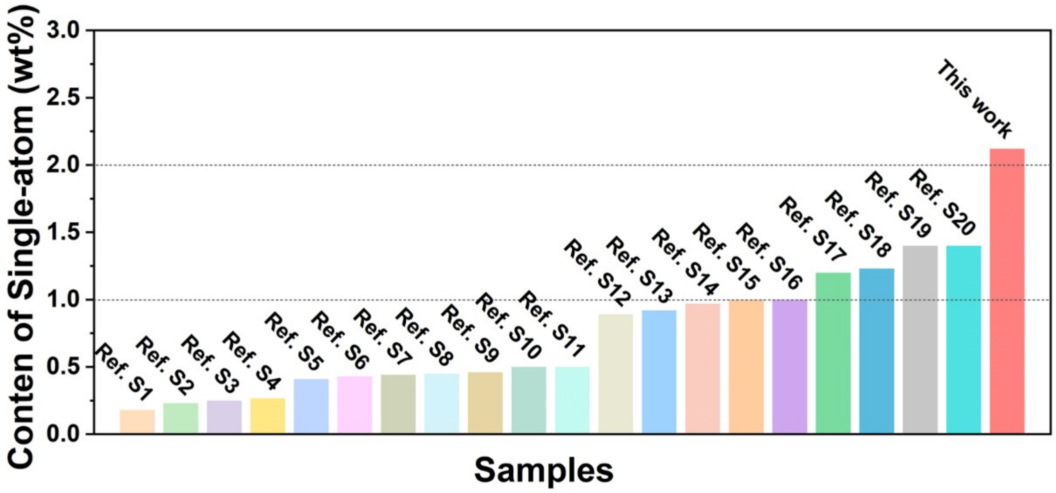

**Fig. S8.** Comparison of metal sing-atom content for CoN5 SA/NC with reported single-atom composites.

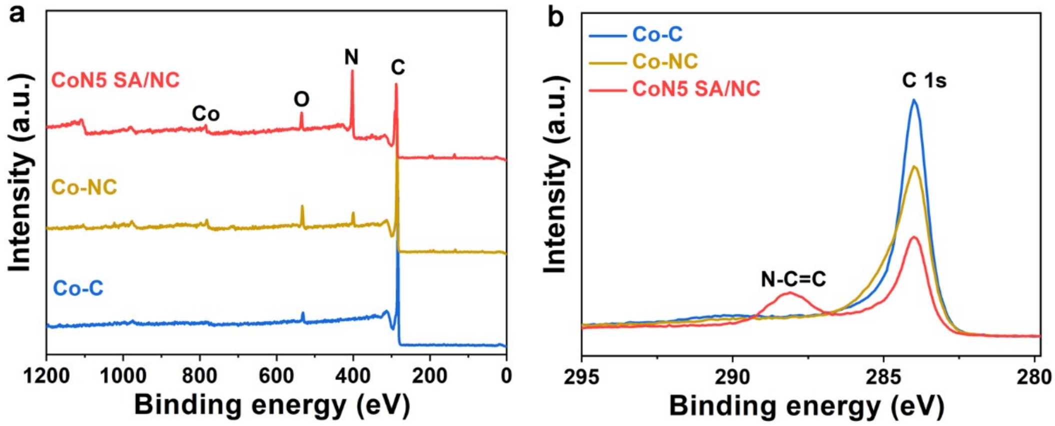

**Fig. S9.** (a) Full survey XRD spectrums, (b) high-resolution C 1s XPS spectra of Co-C, Co-NC, and CoN5 SA/NC

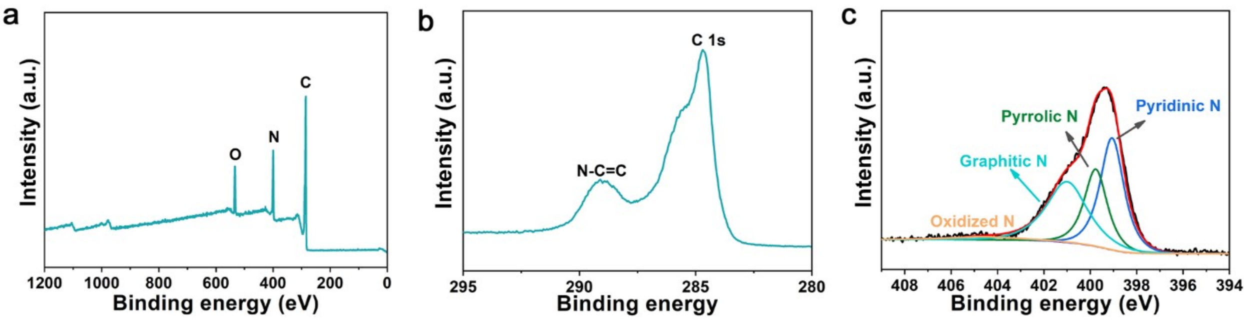

**Fig. S10**. (a) Full survey XPS, (b) High-resolution C 1s and N 1s XPS spectrums for NC.

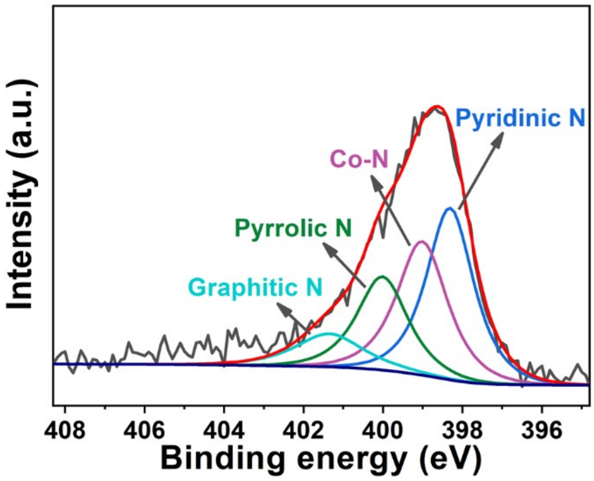

**Fig. S11.** High-resolution N 1s XPS spectrum for Co-NC

**Fig. S12.** Magnetic adsorption effects of (a) Co-C, (b) Co-NC and (c) CoN5 SA/NC. Magnetic adsorption effect of Co-C can be observed when the sample is closed to a powerful magnet. Movie S1 also presents the magnetic adsorption effect of Co-C. However, no similar phenomena may be found for Co-NC (Movie S2) and CoN5 SA/NC (Movie S3), indicating abundant Co atoms are bonded to heteroatom N leading to special magnetic properties, which are different from that of Co-C.

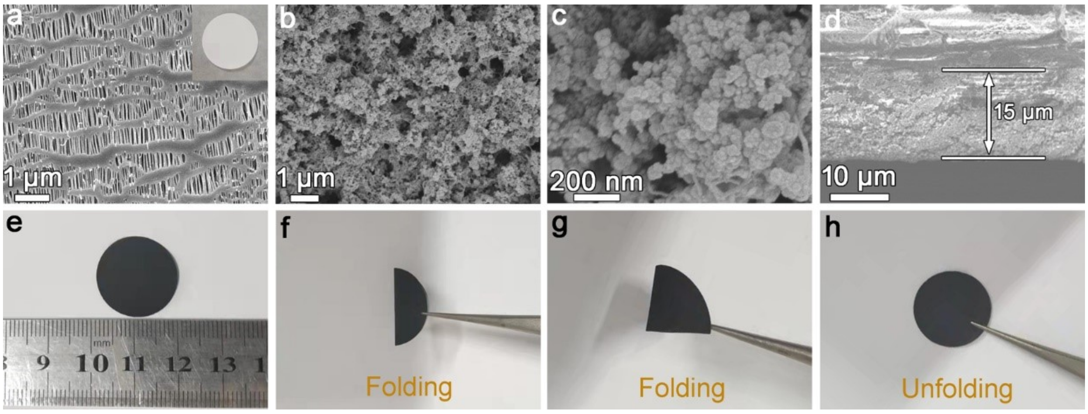

**Fig. S13.** (a) SEM image of commercial PP with inset of the photograph. (b-d) SEM images of CoN5 SA/NC modified PP separator. (e-h) Digital photos of CoN5 SA/NC modified PP separator at folding or unfolding state. The commercial polypropylene (PP) separator (Celgard-2500) owns slit nanopores of around several-hundred nanometres.

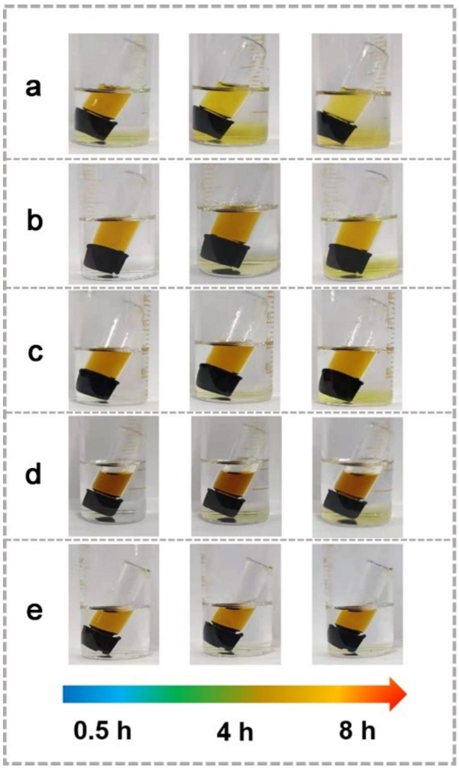

**Fig. S14.** Polysulfide diffusion tests for (a) PP separator, (b) NC modified PP separator, (c) Co-C modified PP separator, (d) Co-NC modified PP separator and (e) Co-N5 SA/NC modified PP separator.

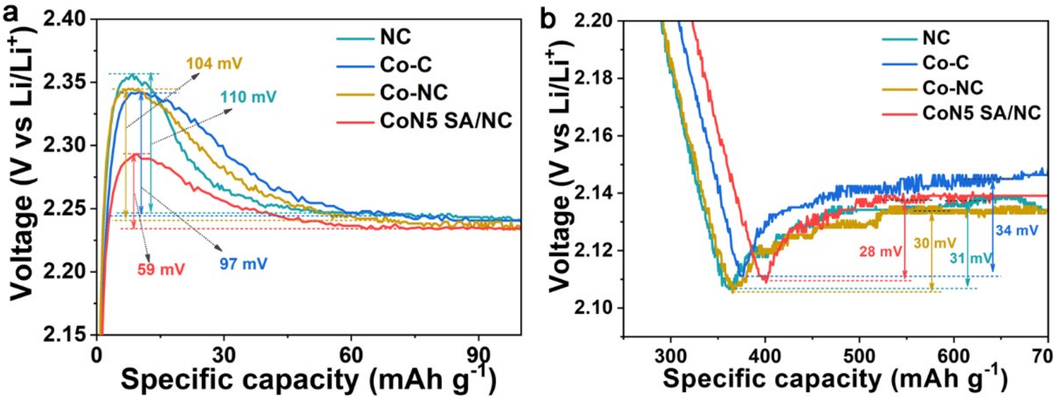

**Fig. S15.** (a) Charge and (b) discharge profiles of cells with NC, Co-C, Co-NC, and CoN5 SA/NC modified separators, respectively, revealing the different overpotentials for conversion between insoluble $Li_2S_2$/$Li_2S$ and soluble LiPSs over the catalysts

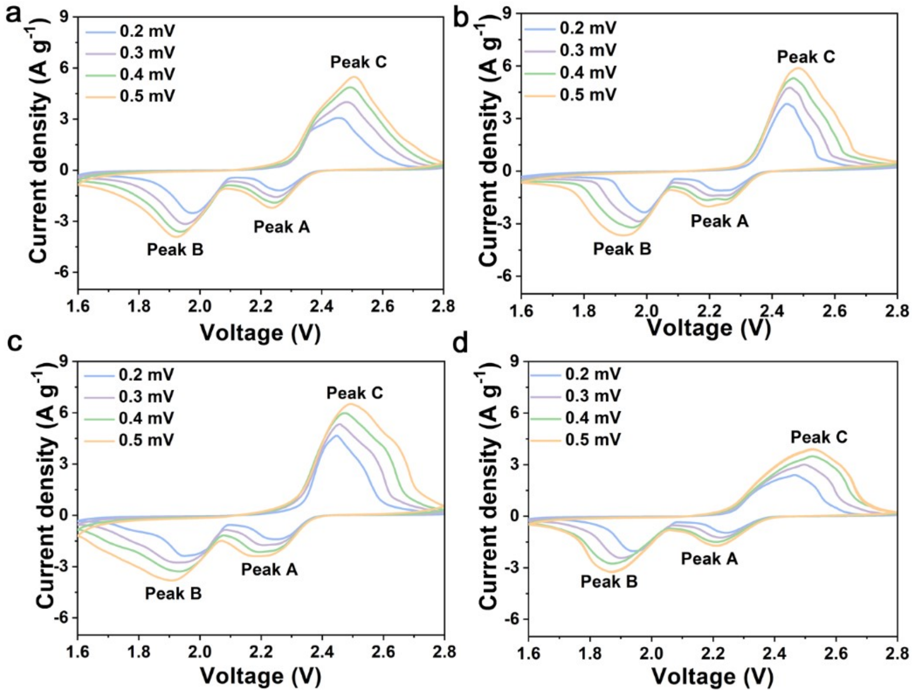

**Fig. S16.** CV curves of the electrodes with (a) Co-NC, (b) Co-C, (c) NC and (d) PP modified separators at various scanning rates.

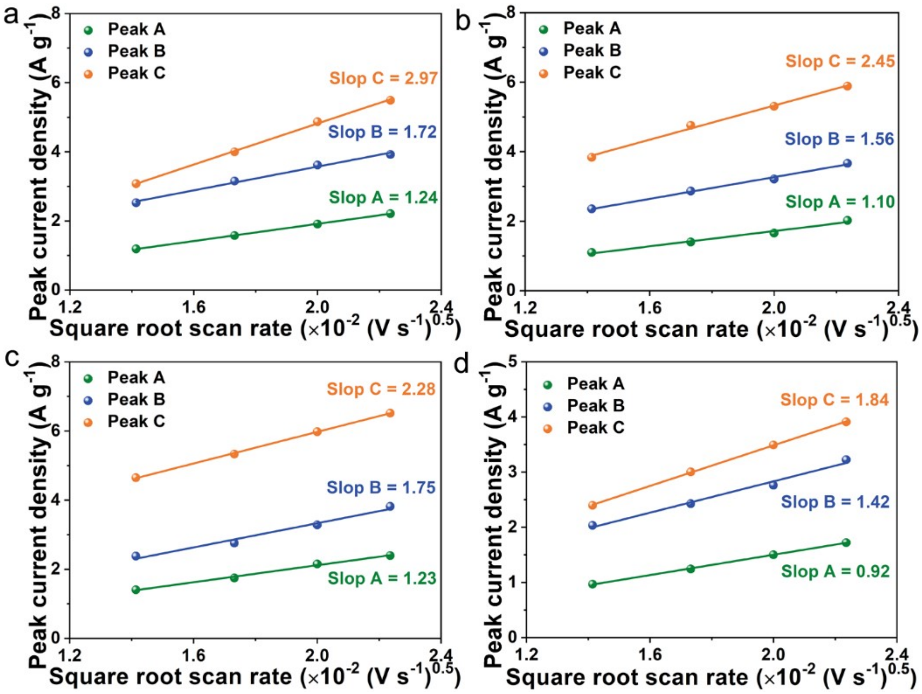

**Fig. S17.** CV current values of peaks A, B, and C for the cells based on (a) Co-NC, (b) Co-C, (c) Co-NC and (d) PP versus square root of scan rates. The Peaks A, B and C are corresponding to Figure S15. The $Li^+$ diffusion coefficients ($D_{Li+}$) can be evaluated using the Randles-Sevcik equation (S2):

$$I_p = \left(2.69\times10^5\right) n^{1.5} A D_{Li^+}{}^{0.5} C_{Li^+} v^{0.5} \qquad \text{(S2)}$$

where, $I_P$ represents the current peak density, $n$ is the electron transferred number, $A$ corresponds to the area of the electrode, $C_{Li+}$ is the concentration of $Li^+$, and $v$ is the sweep rate.

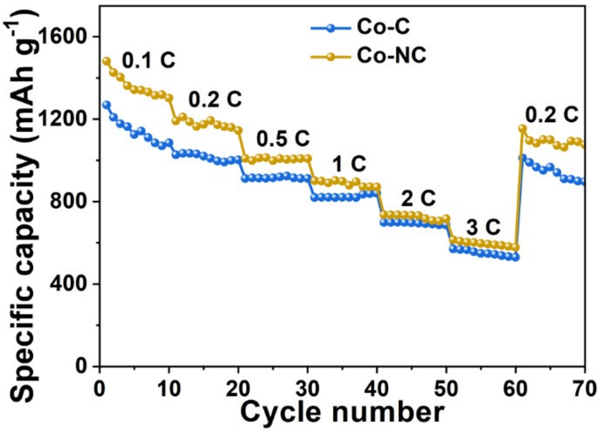

**Fig. S18.** Comparison of the rate performances for the cells with Co-C and Co-NC modified separators. The cell with Co-NC modified separator delivers the capacities of 1481, 1165, 1012, 898, 732 and 587 mAh $g^{-1}$ at 0.1 C, 0.2 C, 0.5 C, 1 C, 2 C and 3 C, respectively. The cell with Co-C modified separator delivers the capacities of 1269, 1031, 914, 820, 695 and 538 mAh $g^{-1}$ at 0.1 C, 0.2 C, 0.5 C, 1 C, 2 C and 3 C, respectively.

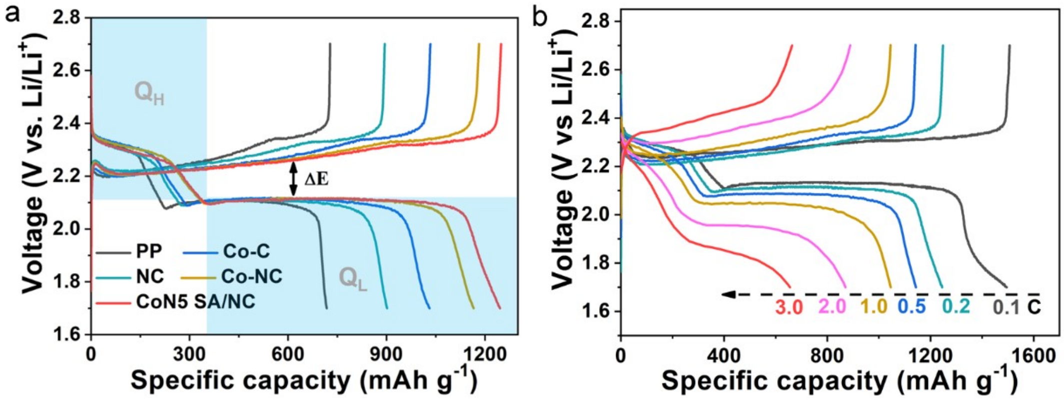

**Fig. S19.** (a) Charging and discharging curves of different electrodes at 0.2 C. (b) Galvanostatic discharge-charge profiles of CoN5 SA/NC-based cell at various current rates from 0.1 to 3 C.

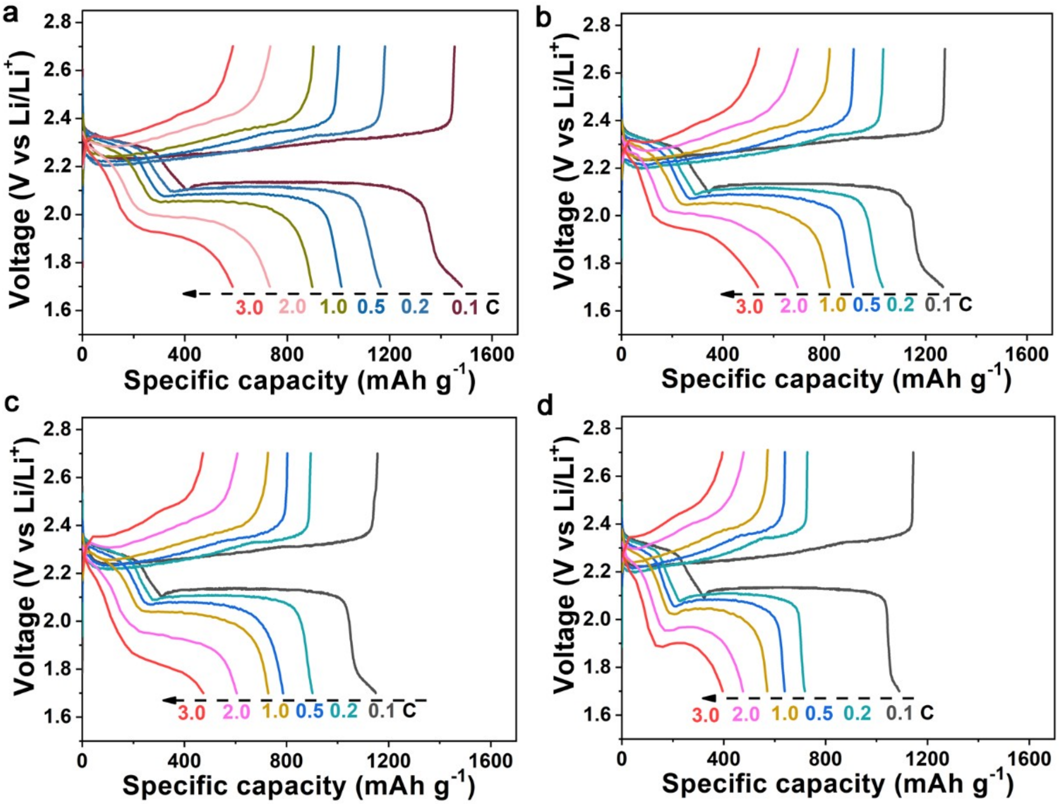

**Fig. S20.** Galvanostatic discharge-charge profiles of cells with (a) Co-NC, (b) Co-C, (c) NC and (d) PP modified separators at various current rates from 0.1 to 3 C.

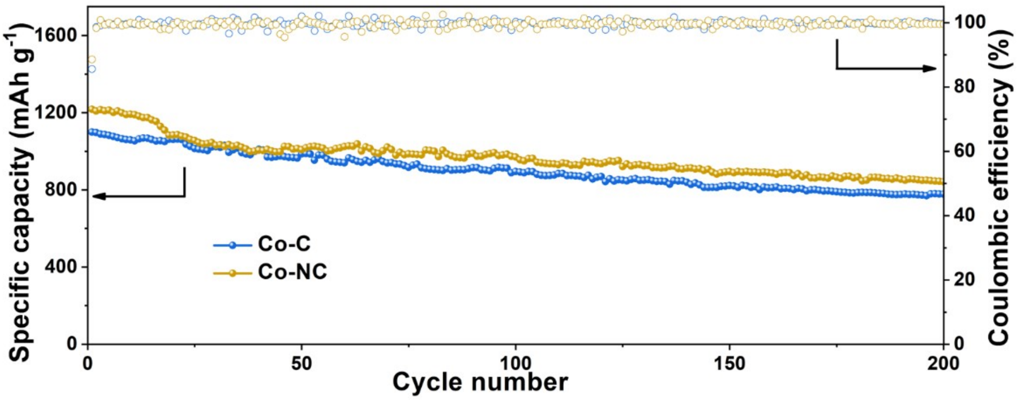

**Fig. S21.** Cycling performances of cells with (a) Co-C and (b) Co-NC modified separators at 0.5 C.

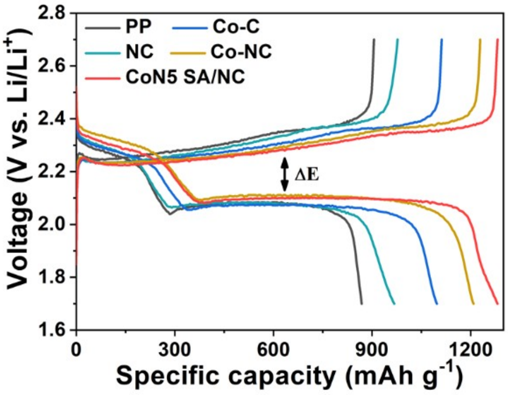

**Fig. S22.** Charging and discharging curves of different electrodes of initial cycle at a current rate of 0.5 C.

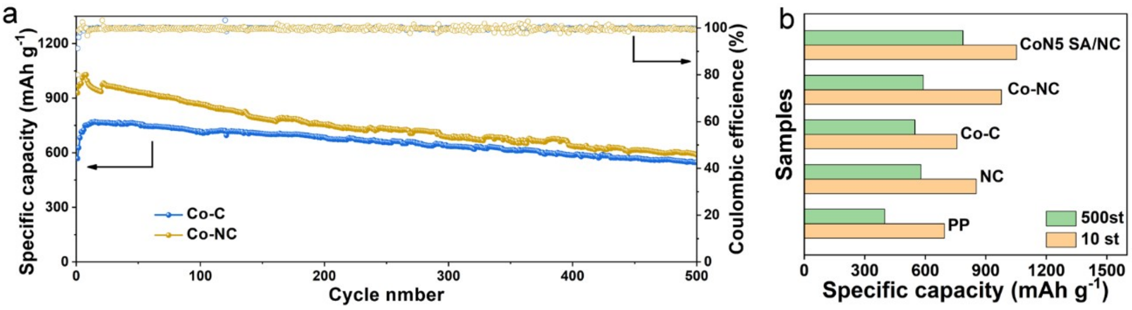

**Fig. S23.** Cycling performances of cells with (a) Co-C and Co-NC modified separators at 1 C. (b) Comparison of the cycling capacity for different electrodes at 1 C after 10th and 500th cycles, respectively.

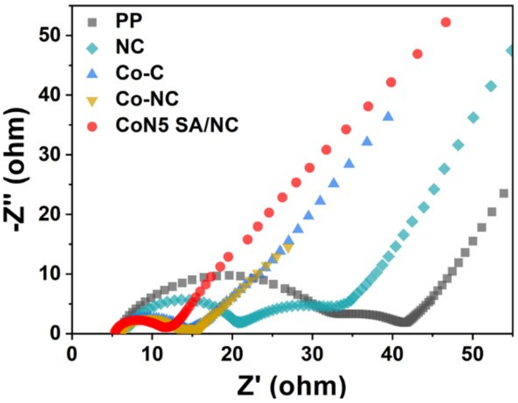

**Fig. S24.** Electrochemical impedance spectroscopy (EIS) plots of the all cells after 500 cycles.

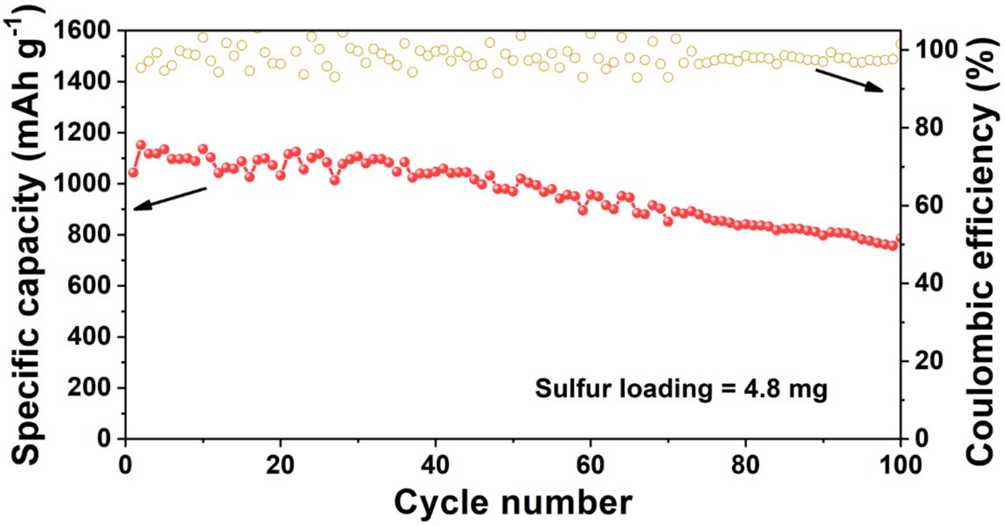

**Fig. S25.** Cycling performance of the cell based CoN5 SA/NC with a high sulfur loading of 4.8 mg at 0.2 C.

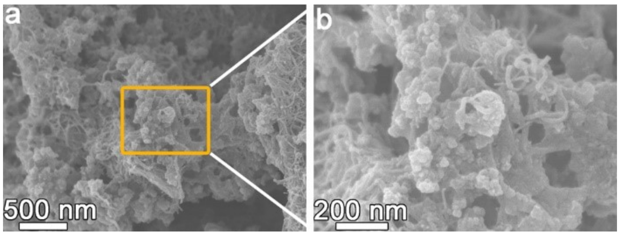

**Fig. S26.** (a,b) SEM images of sulfur/CoN5 SA/NC cathode after tense cycles.

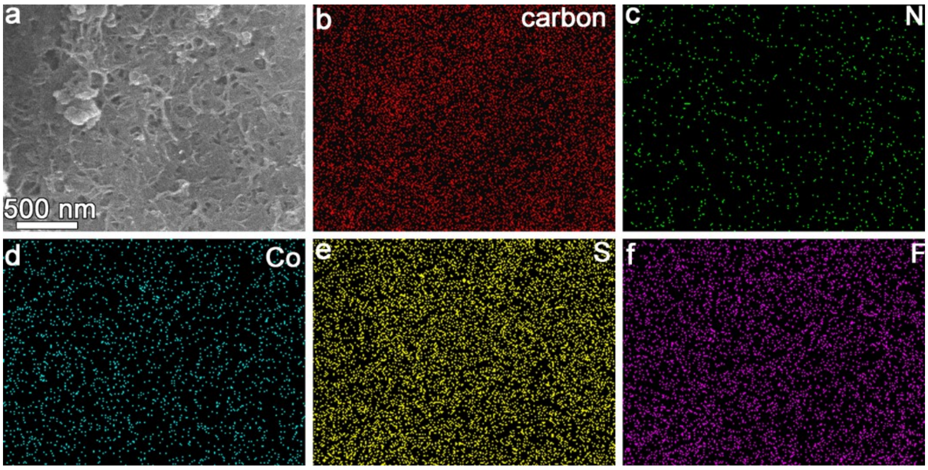

**Fig. S27.** (a) SEM and (b-f) elemental mapping images of sulfur/CoN5 SA/NC cathode after intense cycles: (b) carbon, (c) N, (d) Co, (e) S and (f) F.

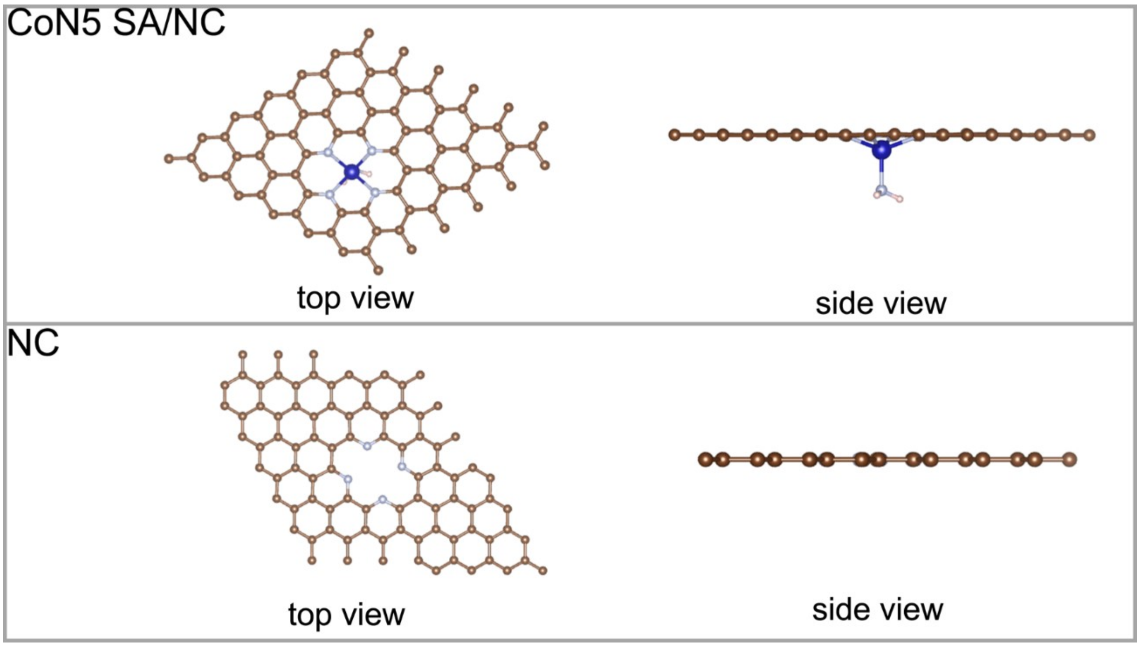

**Fig. S28.** Top and side views of optimized conformations for CoN5 SA/NC and NC. The blue, blue grey, brown and rose red balls represent Co, N, C and H atoms, respectively.

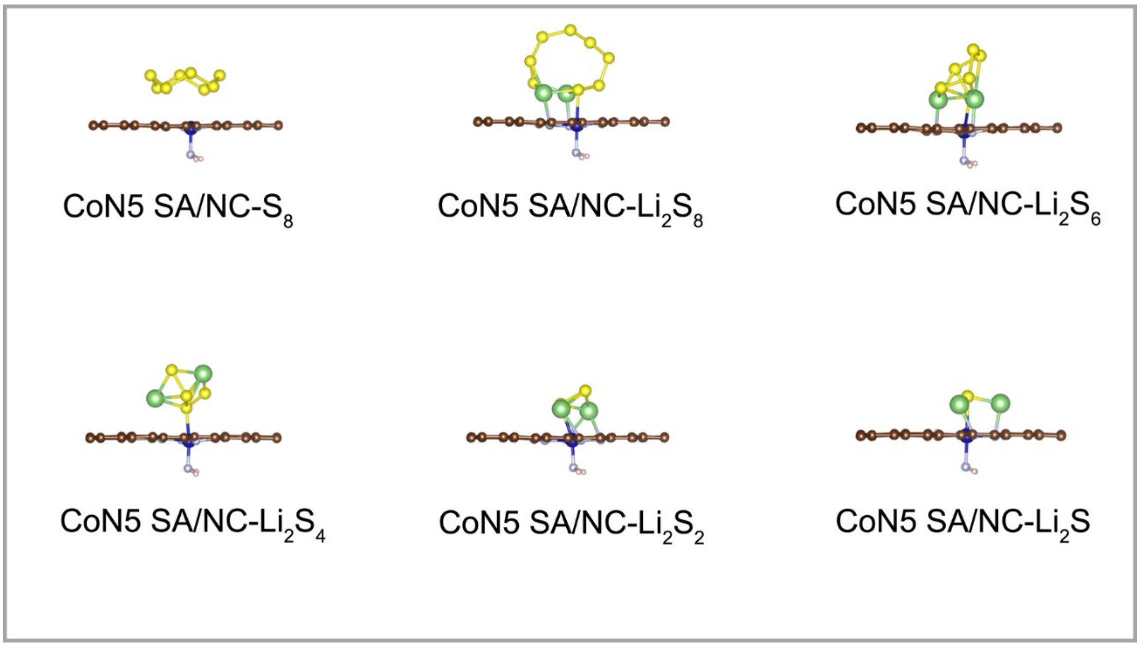

**Fig. S29.** Side views of optimized adsorption conformations of sulfur species on CoN5 SA/NC substrate. The blue, blue grey, brown, rose red, green and yellow balls represent Co, N, C, H, Li and S atoms, respectively.

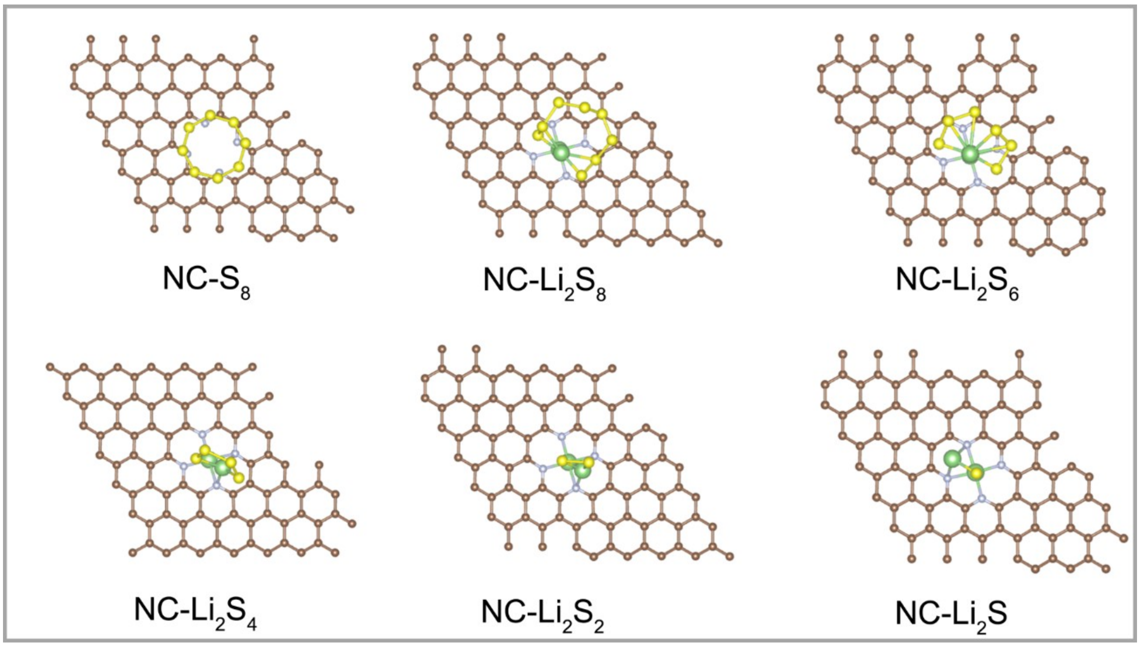

**Fig. S30.** Top views of optimized adsorption conformations of sulfur species on NC substrate. The blue grey, brown, green and yellow balls represent N, C, Li and S atoms, respectively.

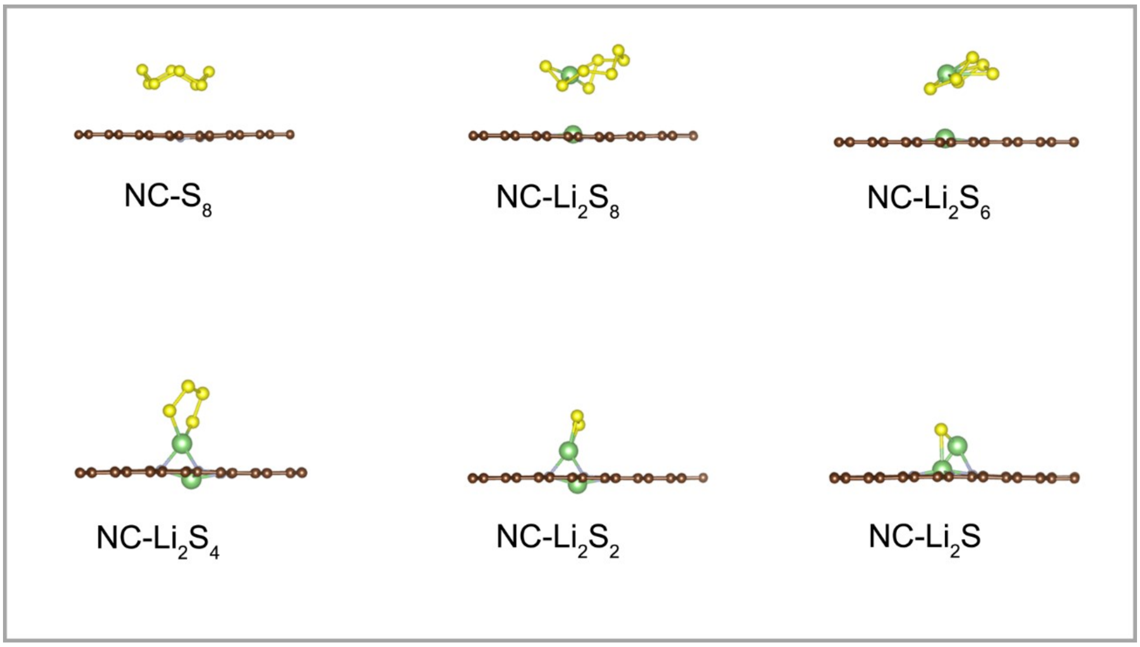

**Fig. S31.** Side views of optimized adsorption conformations of S species on NC substrate. The blue grey, brown, green and yellow balls represent N, C, Li and S atoms, respectively.

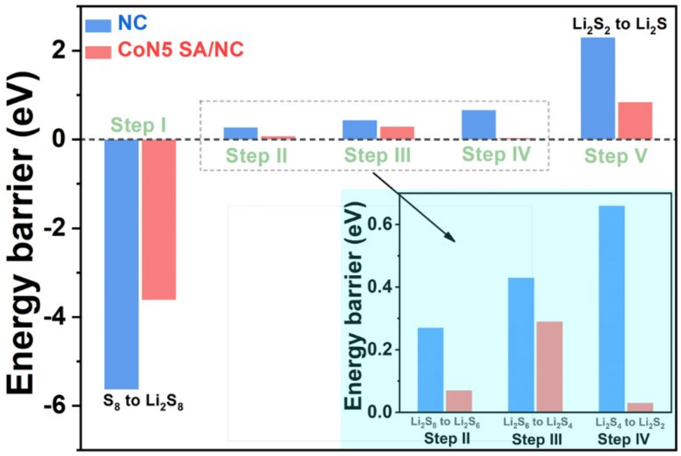

**Fig. S32**. Comparison of the energy barrier for CoN5 SA/NC and NC.

## *Supplementary Tables*

**Table S1.** Porosity Properties of CoN5 SA/NC and reference samples.

| Sample | $S_{BET}$ ($m^2$ $g^{-1}$) | $V_{total}$ ($cm^3$ $g^{-1}$) |
|---|---|---|
| AC | 233 | 0.45 |
| Co-NC | 115 | 0.27 |
| CoN5 SA/NC | 112 | 0.39 |

**Table S2.** Inductively coupled plasma optical emission spectrometry (ICP-OES) results for the Co-C, Co-NC and CoN5 SA/NC samples.

| Sample | Co wt% |
|---|---|
| Co-C | 4.15 |
| Co-NC | 1.94 |
| CoN5 SA/NC | 2.12 |

**Table S3.** Comparison of the metal single-atom (SA) content for the CoN5 SA/NC catalyst in this work with other reported SA electrocatalysts.

| Entry | SA electrocatalysts | Metal SA content (wt%) | Ref. |
|---|---|---|---|
| 1 | $CoN_x$/G | 0.18 | S1 |
| 2 | Co-SNC | 0.23 | S2 |
| 3 | Fe/SNCFs-$NH_3$ | 0.25 | S3 |
| 4 | $Fe_2$-$N_6$-C-p | 0.267 | S4 |
| 5 | O-Fe-N-C | 0.41 | S5 |
| 6 | 2Bn-Cu@UiO-67 | 0.43 | S6 |
| 7 | Cu-CDs | 0.44 | S7 |
| 8 | $Co_1$/NPC | 0.45 | S8 |
| 9 | $H_2$-$FeN_4$/C | 0.459 | S9 |
| 10 | Co-CMS | 0.5 | S10 |
| 11 | Ru-SAS/SNC | 0.5 | S11 |
| 12 | Ni-$N_4$-O | 0.89 | S12 |
| 13 | SA-Rh/CN | 0.92 | S13 |
| 14 | In SAs/NSC | 0.97 | S14 |
| 15 | Co-NC | 1.0 | S15 |
| 16 | Pd/N&F-C | 1.0 | S16 |
| 17 | $Ir_1$/CN | 1.2 | S17 |
| 18 | 3d-omsh/ZnS, Co-N-C | 1.23 | S18 |
| 19 | Co SAs/BCN | 1.4 | S19 |
| 20 | $Co_1$-NG(O) SACs | 1.4 | S20 |
| **21** | **CoN5 SA/NC** | **2.12** | **This work** |

**Table S4**. The atomic ratios of nitrogen species in CoN5 SA/NC, Co-NC and NC samples are calculated by XPS.

| Sample | Pyridinic-N (at.%) | Co-N (at.%) | Pyrrolic-N (at.%) | Graphitic-N (at.%) | Oxidized-N (at.%) | In total (at.%) |
|---|---|---|---|---|---|---|
| NC | – | 6.3 | 4.2 | 5.9 | 0.4 | 16.8 |
| Co-NC | 2.3 | 2.7 | 1.6 | 0.7 | – | 7.3 |
| CoN5 SA/NC | 11.9 | 7.1 | 6.5 | 2.9 | 1.6 | 30.0 |

**Table S5.** EXAFS fitting parameters at the Co K-edge for CoN5 SA/NC.

| Sample | Shell | N [a] | R (Å) [b] | $\sigma^2$ (Å$^2$·10$^{-3}$) [c] | $\Delta E_0$ (eV) [d] | R factor (%) |
|---|---|---|---|---|---|---|
| CoN5 SA/NC | Co-N | 5.2 | 2.07 | 9.2 | -1.0 | 0.2 |

[a] N: coordination numbers; [b] R: bond distance; [c] $\sigma^2$: Debye-Waller factors; [d] $\Delta E_0$: the inner potential correction. And R factor: goodness of fit. The error bounds (accuracies) of the above the structural parameters are estimated as N, ± 20%; R, ± 1%; $\sigma^2$ ± 20%; and $\Delta E_0$, ± 20%.

**Table S6.** Comparison of the electrochemical performance of Li-S batteries with high sulfur loading.

| Samples | Rate (C) | Sulfur loading (mg cm$^{-2}$) | Initial capacity (mAh g$^{-1}$) | Cycle number | Retained capacity (mAh g$^{-1}$) | Ref. |
|---|---|---|---|---|---|---|
| HFeNG | 0.1 | 5.0 | 5.0 | 100 | 3.8 | S21 |
| SC-Co | 0.1 | 3.6 | 4.1 | 100 | 3.0 | S22 |
| Gh/FePc+OFN | 0.1 | 4.0 | 2.7 | 150 | 2.2 | S23 |
| Fe-N/MHCS | 0.1 | 5.4 | 6.42 | 100 | 5.24 | S24 |
| Co-PCNF | 0.1 | 6.9 | 7.15 | 50 | 6.4 | S25 |
| SA-Fe/$Fe_2N$@NG | 0.1 | 5.0 | 6.0 | 100 | 5.02 | S26 |
| Ni−$N_5$/HNPC | 0.1 | 5.1 | 5.6 | 80 | 4.0 | S27 |
| Ni-MOF-1D | 0.1 | 6.7 | 6.63 | 50 | 5.37 | S28 |
| **CoN5 SA/NC** | **0.1** | **5.4** | **6.12** | **200** | **4.82** | **This work** |
| **CoN5 SA/NC** | **0.1** | **6.5** | **7.25** | **150** | **4.76** | **This work** |

## *Supplementary References*

S1 Q. e. Huang, B. Wang, S. Ye, H. Liu, H. Chi, X. Liu, H. Fan, M. Li, C. Ding, Z. Li and C. Li, *ACS Catal.*, 2022, **12**, 491-496.X

S2 H. Wang, X. Wang, J. Pan, L. Zhang, M. Zhao, J. Xu, B. Liu, W. Shi, S. Song and H. Zhang, *Angew. Chem. Int. Ed.*, 2021, **60**, 23154-23158.

S3 L. Yang, X. Zhang, L. Yu, J. Hou, Z. Zhou and R. Lv, *Adv. Mater.*, 2022, **34**, 2105410.

S4 Y. Wang, B. J. Park, V. K. Paidi, R. Huang, Y. Lee, K.-J. Noh, K.-S. Lee and J. W. Han, *ACS Energy Lett.*, 2022, **7**, 640-649.

S5 T. Zhang, X. Han, H. Liu, M. Biset-Peiró, J. Li, X. Zhang, P. Tang, B. Yang, L. Zheng, J. R. Morante and J. Arbiol, *Adv. Funct. Mater.*, 2022, **32**, 2111446.

S6 S. Chen, W.-H. Li, W. Jiang, J. Yang, J. Zhu, L. Wang, H. Ou, Z. Zhuang, M. Chen, X. Sun, D. Wang and Y. Li, *Angew. Chem. Int. Ed.*, 2022, **61**, e202114450.

S7 Y. Cai, J. Fu, Y. Zhou, Y.-C. Chang, Q. Min, J.-J. Zhu, Y. Lin and W. Zhu, *Nat. Commun.*, 2021, **12**, 586.

S8 H. Jin, P. Li, P. Cui, J. Shi, W. Zhou, X. Yu, W. Song and C. Cao, *Nat. Commun.*, 2022, **13**, 723.

S9 C. Liu, Y. Wu, K. Sun, J. Fang, A. Huang, Y. Pan, W.-C. Cheong, Z. Zhuang, Z. Zhuang, Q. Yuan, H. L. Xin, C. Zhang, J. Zhang, H. Xiao, C. Chen and Y. Li, *Chem*, 2021, **7**, 1297-1307.

S10 S. Liang, L.-C. Zou, L.-J. Zheng, F. Li, X.-X. Wang, L.-N. Song and J.-J. Xu, *Adv. Energy Mater.*, 2022, **12**, 2103097.

S11 J. Qin, H. Liu, P. Zou, R. Zhang, C. Wang and H. L. Xin, *J. Am. Chem. Soc.*, 2022, **144**, 2197-2207.

S12 X. Zhang, P. Zhai, Y. Zhang, Y. Wu, C. Wang, L. Ran, J. Gao, Z. Li, B. Zhang, Z. Fan, L. Sun and J. Hou, *J. Am. Chem. Soc.*, 2021, **143**, 20657-20669.

S13 Y. Xiong, J. Dong, Z.-Q. Huang, P. Xin, W. Chen, Y. Wang, Z. Li, Z. Jin, W. Xing, Z. Zhuang, J. Ye, X. Wei, R. Cao, L. Gu, S. Sun, L. Zhuang, X. Chen, H. Yang, C. Chen, Q. Peng, C.-R. Chang, D. Wang and Y. Li, *Nat. Nanotechnol.*, 2020, **15**, 390-397.

S14 E. Zhang, L. Tao, J. An, J. Zhang, L. Meng, X. Zheng, Y. Wang, N. Li, S. Du, J. Zhang, D. Wang and Y. Li, *Angew. Chem. Int. Ed.*, 2022, 61, e202117347.

S15 Q. Deng, X. Li, R. Gao, J. Wang, Z. Zeng, J.-J. Zou, S. Deng and S. C. E. Tsang, *J. Am. Chem. Soc.*, 2021, 143, 21294-21301.

S16 J. Chang, G. Wang, M. Wang, Q. Wang, B. Li, H. Zhou, Y. Zhu, W. Zhang, M. Omer, N. Orlovskaya, Q. Ma, M. Gu, Z. Feng, G. Wang and Y. Yang, *Nat. Energy*, 2021, **6**, 1144-1153.

S17 Z. Li, Y. Chen, S. Ji, Y. Tang, W. Chen, A. Li, J. Zhao, Y. Xiong, Y. Wu, Y. Gong, T. Yao, W. Liu, L. Zheng, J. Dong, Y. Wang, Z. Zhuang, W. Xing, C.-T. He, C. Peng, W.-C. Cheong, Q. Li, M. Zhang, Z. Chen, N. Fu, X. Gao, W. Zhu, J. Wan, J. Zhang, L. Gu, S. Wei, P. Hu, J. Luo, J. Li, C. Chen, Q. Peng, X. Duan, Y. Huang, X.-M. Chen, D. Wang and Y. Li, *Nat. Chem.*, 2020, **12**, 764-772.

S18 C. Zhao, G.-L. Xu, Z. Yu, L. Zhang, I. Hwang, Y.-X. Mo, Y. Ren, L. Cheng, C.-J. Sun, Y. Ren, X. Zuo, J.-T. Li, S.-G. Sun, K. Amine and T. Zhao, *Nat. Nanotechnol.*, 2021, **16**, 166-173.

S19 Y. Min, X. Zhou, J.-J. Chen, W. Chen, F. Zhou, Z. Wang, J. Yang, C. Xiong, Y. Wang, F. Li, H.-Q. Yu and Y. Wu, *Nat. Commun.*, 2021, **12**, 303.

S20 E. Jung, H. Shin, B.-H. Lee, V. Efremov, S. Lee, H. S. Lee, J. Kim, W. Hooch Antink, S. Park, K.-S. Lee, S.-P. Cho, J. S. Yoo, Y.-E. Sung and T. Hyeon, *Nat. Mater.*, 2020, **19**, 436-442.

S21 Y. Wang, D. Adekoya, J. Sun, T. Tang, H. Qiu, L. Xu, S. Zhang and Y. Hou, *Adv. Funct. Mater.*, 2019, **29**, 1807485.

S22 J. Xie, B.-Q. Li, H.-J. Peng, Y.-W. Song, M. Zhao, X. Chen, Q. Zhang and J.-Q. Huang, *Adv. Mater.*, 2019, **31**, 1903813.

S23 S. Zhou, S. Yang, X. Ding, Y. Lai, H. Nie, Y. Zhang, D. Chan, H. Duan, S. Huang and Z. Yang, *ACS Nano*, 2020, **14**, 7538-7551.

S24 Q. Shao, L. Xu, D. Guo, Y. Su and J. Chen, *J. Mater. Chem. A*, 2020, **8**, 23772-23783.

S25 T. Huang, Y. Sun, J. Wu, J. Jin, C. Wei, Z. Shi, M. Wang, J. Cai, X.-T. An, P. Wang, C. Su, Y.-y. Li and J. Sun, *ACS Nano*, 2021, **15**, 14105-14115.

S26 C. Ma, Y. Zhang, Y. Feng, N. Wang, L. Zhou, C. Liang, L. Chen, Y. Lai, X. Ji, C. Yan and W. Wei, *Adv. Mater.*, 2021, **33**, 2100171.

S27 S. Zhang, X. Ao, J. Huang, B. Wei, Y. Zhai, D. Zhai, W. Deng, C. Su, D. Wang and Y. Li, *Nano Lett.*, 2021, **21**, 9691-9698.

S28 D. Yang, Z. Liang, P. Tang, C. Zhang, M. Tang, Q. Li, J. J. Biendicho, J. Li, M. Heggen, R. E. Dunin-Borkowski, M. Xu, J. Llorca, J. Arbiol, J. R. Morante, S.-L. Chou and A. Cabot, *Adv. Mater.*, 2022, **34**, 2108835.